Journal of Power Sources 696 (2026) 241495

Contents lists available at ScienceDirect

Journal of Power Sources

journal homepage: www.elsevier.com/locate/jpowsour

An accelerated method for determining the solid-phase diffusion coefficient and reaction-rate constant for Li-ion batteries

Haider Adel Ali Ali [a,b], Luc H.J. Raijmakers [a,*], Anna Windmüller [a], Hermann Tempel [a], Boryann Liaw [a,c], Peter H.L. Notten [a,d,e], Rüdiger-A. Eichel [a,b]

[a] Forschungszentrum Jülich GmbH, Institute of Energy Technologies (IET-1), Wilhelm-Johnen-Straße, Jülich, 52428, Germany
[b] RWTH Aachen University, Institute of Physical Chemistry, Landoltweg 2, Aachen, 52074, Germany
[c] High Power Research Laboratory, LLC, Sparks, NV, 89436, USA
[d] Eindhoven University of Technology, P.O. Box 513, Eindhoven, MB, 5600, the Netherlands
[e] Centre for Clean Energy Technology, University of Technology Sydney, Broadway, Sydney, NSW, 2007, Australia

HIGHLIGHTS

- Accelerated GITT method reduces measurement time by up to 95 %.
- A 10 mV h^{-1} cutoff balances speed and agreement with the 6 h reference.
- ESPM successfully replaces DFN for faster parameter optimization.
- Ten-minute rests yield D_s and k_0 close to 6 h estimates and similar voltage errors.

ARTICLE INFO

Keywords:
Batteries
Li-ion batteries
Battery modelling
DFN model
ESPM
Model parameterization

ABSTRACT

This study presents an approach to accelerate galvanostatic intermittent titration technique (GITT) measurements for determining the solid-phase diffusion coefficient (D_s) and reaction-rate constant (k_0) used in physics-based battery models such as the Doyle-Fuller-Newman (DFN) model. The approach addresses the challenge of lengthy measurement times associated with conventional GITT protocols. By using the DFN model to predict cell states during battery operation, the proposed method reduces the relaxation duration to 10 min while retaining close agreement with the D_s and k_0 estimates obtained using a 6 h-relaxation reference protocol and comparable voltage-prediction performance in separate constant-current and dynamic load profile validations. Additionally, terminating the relaxation when the voltage relaxation rate threshold falls below 10 mV h^{-1} reduces the total GITT measurement time by 95 %. The study also demonstrates that the extended single particle model (ESPM) provides an efficient alternative to the DFN model for the determination of D_s and k_0, reducing computational requirements while providing comparable parameter estimates. These findings accelerate physics-based model parameterization, facilitating faster cell development and improving the accessibility of electrochemical parameters.

1. Introduction

Li-ion batteries (LIBs) are complex electrochemical devices and the ability to understand their internal processes is important for improving performance and design, as well as for ensuring safe operation [1–3]. Mathematical models that capture the fundamental electrochemical and physical processes occurring within the battery are very suitable for understanding these complex internal processes. Among the various existing models, physics-based approaches, most notably the Doyle-Fuller-Newman (DFN) model have proven to be effective tools due to their ability to simulate the various (local) internal states in batteries [4,5].

To use the DFN model effectively, it must be accurately parameterized. In principle, model parameters should be determined experimentally wherever possible and directly implemented into the model, ensuring a clear physical meaning. In practice, however, not all

* Corresponding author.
E-mail address: l.raijmakers@fz-juelich.de (L.H.J. Raijmakers).

https://doi.org/10.1016/j.jpowsour.2026.241495
Received 3 May 2026; Received in revised form 25 August 2026; Accepted 9 September 2026
Available online 19 September 2026
0378-7753/© 2026 The Authors. Published by Elsevier B.V. This is an open access article under the CC BY license (http://creativecommons.org/licenses/by/4.0/).
Open access funding enabled and organized by Projekt DEAL.

parameters can be measured directly, and optimization procedures are then commonly employed to identify parameter values that reproduce measured cell behavior [6–10]. For parameters that are experimentally inaccessible or insufficiently constrained by available data, assumptions or literature values are sometimes required, although these introduce additional uncertainty and should therefore be minimized and explicitly documented.

Two key parameters that significantly influence LIB operating performance and internal state prediction are the solid-phase diffusion coefficient (D_s) and the reaction-rate constant (k_0). These two parameters cannot be directly measured and require parameter optimization [9, 11–16]. Based on previous work [17], the combination of galvanostatic intermittent titration technique (GITT) measurements with the DFN model has been identified as an effective approach for estimating D_s and k_0. Simulation results from the DFN model with the optimized parameters show very good agreement with measurements under both constant current (CC) discharge at various current densities and dynamic load profiles. However, a drawback of this method is the relatively long duration of GITT measurements, as the existing approach requires the cell voltage to fully relax to a steady state before starting the next GITT pulse. As a result, a complete parameterization experiment can take more than one week [17,18], limiting the practicality of GITT for routine battery characterization and model parameterization. Relaxation durations are particularly long at low temperatures and/or for electrode materials with low diffusion coefficients, and it is obvious that long measurement durations are not particularly advantageous for accelerated battery development.

To circumvent the long duration of traditional GITT, several rapid diagnostic frameworks have been proposed. For instance, Chien et al. [13] introduced the Intermittent Current Interruption (ICI) method to determine D_s rapidly during continuous cycling, while Gümrükçüoğlu et al. [15] developed a so-called Inference from a Consistent Model (ICM) approach that extracts diffusivity directly from transient non-equilibrium data. However, these approaches focus primarily on isolating D_s and do not account for k_0. More recently, Mebane et al. [19] introduced an embedded machine learning methodology using Gaussian process regression to predict full relaxation behavior from early-stage transients. While data-driven methods offer fast predictions, they can rely heavily on substantial reference datasets for model training and generalization.

In addition, the computational effort associated with parameter optimization using physics-based models can be reduced by replacing the DFN model with the extended single particle model (ESPM), a reduced-order electrochemical model that is well suited to the low-to-intermediate current conditions typically employed during GITT measurements [20–23]. The ESPM is suitable for use in combination with GITT measurements, as these are typically performed at low to intermediate currents [16,20,21].

In this work, an accelerated GITT parameterization workflow using shortened relaxation durations is proposed to reduce measurement time. The method retains the simulated solid- and electrolyte-phase concentration states between consecutive GITT intervals, thereby enabling parameter estimation without requiring full relaxation after every pulse. The shortened protocols are evaluated according to two distinct criteria: (i) agreement of the inferred D_s and k_0 profiles with those obtained using a 6 h relaxation protocol under the same model-based estimation procedure and (ii) voltage-prediction performance in separate constant-current and dynamic load profile validations. In addition to fixed relaxation durations, the rate of cell-voltage change during rest is evaluated as an adaptive criterion for terminating each relaxation period. Finally, the ESPM is compared with the DFN model as a reduced-order alternative for decreasing the computational effort for D_s and k_0 determination.

2. Theoretical considerations

A typical half cell, as schematically shown in Fig. 1a, consists of a current collector, porous positive electrode (pos), a separator (sep), and counter electrode (Li-metal foil), filled with a liquid electrolyte. In Fig. 1a, the active material of the positive electrode is illustrated as green particles. The small reddish and bluish particles represent additives and binders, respectively. Fig. 1b illustrates the DFN model, which is based on porous electrode theory. In this DFN model, the positive electrode is assumed to be a collection of uniform spherical particles of identical size.

The DFN model simulates the dynamics within the battery cell in two dimensions. The first dimension, denoted as the x-dimension, spans across the thickness of the positive electrode and the separator at a macroscopic scale. The DFN model simulates the mass transfer and electric potential in both the solid and electrolyte-phases across the different layers, including the positive electrode thickness (δ_{pos}) and separator thickness (δ_{sep}), but without the current collectors and the counter electrode. The total thickness of the modelled region is denoted by L. The second dimension, referred to as the r-dimension, considers the microscopic scale, representing the (average) particle radius (R_s) of the positive electrode, derived from its particle-size distribution. A significant simplification can be made by representing solid-phase diffusion in

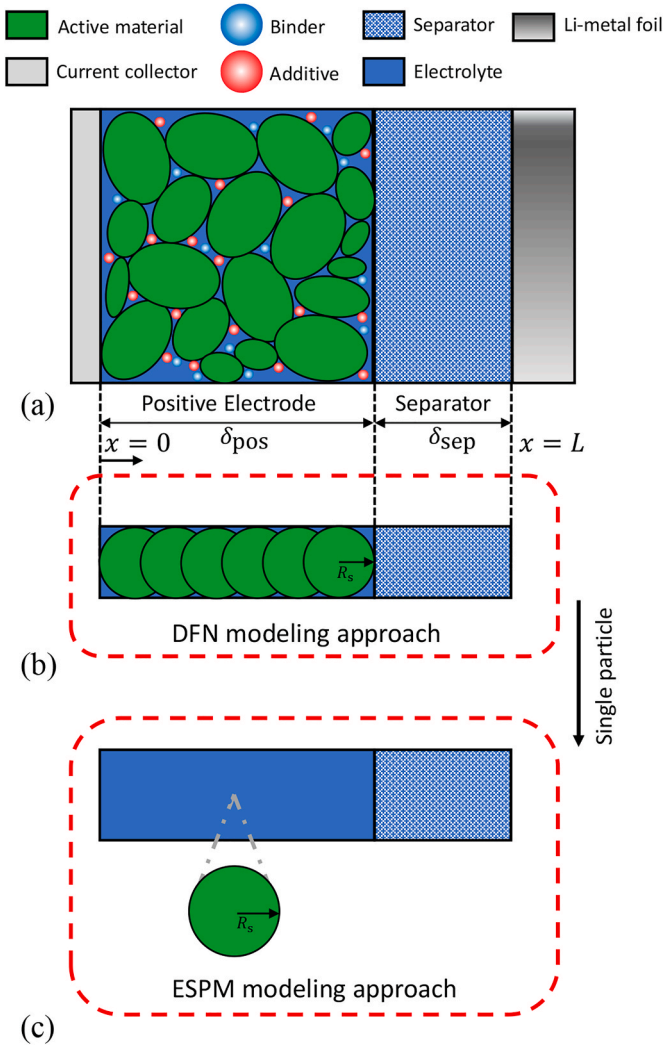


Fig. 1. Schematic illustration of a half-cell (a), the DFN model (b) and the ESPM (c). Parts of this figure were reproduced from Ref. [17] under the Creative Commons Attribution 4.0 license.

the porous positive electrode using a single representative spherical particle, reducing the DFN model to the ESPM, as shown in Fig. 1c. This approach significantly reduces the computational time [20,23].

2.1. DFN model

The DFN model is a widely used physics-based model for LIBs. This study uses a half-cell formulation of the model, governed by the set of partial differential equations (PDEs) shown in Table 1. In the DFN model, the concentration and potential in both the solid and electrolyte-phases are calculated along the x-dimension and the r-dimension, as shown in Eqs. (1)–(4). These four PDEs are coupled via the Butler-Volmer equation in Eq. (5a), which is used to describe the electrochemical reaction at the particle/electrolyte interface. Eqs. (5b-c) are used for calculating the electrode overpotential and exchange current density, respectively. In this work, both D_s (Eq. (1)) and k_0 (Eq. (5c)) are treated as lithiation-dependent, locally (mathematically) optimized parameters, representing the effective solid-phase transport coefficient and kinetic prefactor, respectively, rather than single invariant material constants. During the optimization of a GITT pulse (N), D_s and k_0 in Eqs. (1a) and (5c) are assigned the pulse-specific values $D_{s,N}$ and $k_{0,N}$ and are held constant throughout that interval. Furthermore, the cell voltage is calculated with Eq. (6). All the parameter definitions are provided in the list of symbols. The model parameter values other than D_s and k_0 are provided in Table S1.

2.2. ESPM

The ESPM used in this work is a reduced-order half-cell model in which solid-phase diffusion in the porous positive electrode is represented by a single representative spherical particle, derived under the following assumptions:

- The solid-phase lithium concentration (c_s) is assumed to be uniform along the electrode thickness (x-direction).
- The exchange current density (i_0) is assumed to vary only with time and is independent of the spatial coordinate x.
- The anodic (α_a) and cathodic (α_c) charge-transfer coefficients are both assumed to be equal to 0.5.

These approximations neglect particle-to-particle heterogeneity and through-electrode variations in solid-phase concentration and reaction distribution. However, the model retains the x-dependent electrolyte concentration and electrolyte potential described by Eqs. (2) and (4), respectively, while the solid-phase potential equation, Eq. (3), is neglected. Consequently, the electrode overpotential in Eq. (5b) is modified by introducing the mean electrolyte potential (ϕ_e^{mean}). The Butler-Volmer equation, the electrode overpotential and the cell voltage (Eq. (5)) are then reformulated as Eq. 7a, Eq. 7b, Eq. 8, respectively. More details on the differences between the DFN model and ESPM are elaborated in Refs. [20,23,24].

$$j_{Li}(t) = \frac{I_{app}(t)}{A_{surf}\, a_s\, \delta_{pos}\, F}, \tag{7a}$$

$$\eta(t) = \sinh^{-1}\left(\frac{j_{Li}(t)F}{i_0(t)}\right)\frac{RT}{F} + \phi_e^{mean}(t) + R_f j_{Li} F, \tag{7b}$$

$$V(t) = \eta(t) - U(t) - \frac{R_{cc}}{A_{surf}} I_{app}(t), \tag{8}$$

2.3. Determination method for D_s and k_0

2.3.1. Standard method

The standard method for determining both D_s and k_0 is based on previous work [17]. To summarize, the initial lithiation degree of each GITT pulse is first calculated based on the cumulative charged or discharged capacity. Initial D_s and k_0 values for each pulse are assigned to this nominal lithiation degree at the start of the pulse and are assumed to remain constant during the GITT pulse including subsequent relaxation. Second, k_0 is estimated based on the voltage drop within the first second of the current pulse by using a mathematical optimization algorithm. Finally, D_s is mathematically optimized across the full pulse duration including relaxation period by minimizing the difference between the measured and simulated voltage. In the last step, both the initial lithiation degree and k_0 are further refined by adjusting each parameter by ±10 % and ±30 %, respectively, with respect to their initial values. More information on the steps used for the parameter identification process is presented in the SI under the "Parameter optimization algorithm" Section.

In the standard method, the initial concentrations in both the solid-phase (c_s) and electrolyte-phase (c_e) are assumed to be spatially uniform across both the r-dimension and the x-dimension. In other words, the cell is assumed to be at equilibrium at the start of each pulse. This reflects the modeling assumption adopted here that the cell has reached equilibrium after a sufficiently long relaxation period following the preceding GITT pulse, as shown in the schematic voltage-time profile in Fig. 2a. Accordingly, the concentration gradients in the r- and x-directions are assumed to have vanished in the model, as illustrated by the blue-colored schematic half-cell and enlarged particle. This idealized initialization of the model does not exclude the possibility that small residual concentration gradients remain in the experimental cell.

The advantage of this method is that a long relaxation time allows for the estimation of the electrode's equilibrium potential (U), as this can be determined by taking the final point of the voltage relaxation period. However, the method has drawbacks. The main issue is that the

Table 1
Governing equations of the DFN model for a half-cell [17].

Li-ion concentration in solid phase	$\frac{\partial c_s(r,t)}{\partial t} = \frac{D_s}{r^2}\frac{\partial}{\partial r}\left(r^2\frac{\partial c_s(r,t)}{\partial r}\right)$	(1a)
Boundary conditions	$\left.\frac{\partial c_s(r,t)}{\partial r}\right\|_{r=0} = 0, -D_s\left.\frac{\partial c_s(r,t)}{\partial r}\right\|_{r=R_s} = j_{Li}(x,t),$	(1b)
Li-ion concentration in the electrolyte phase	$\varepsilon_e\frac{\partial c_e(x,t)}{\partial t} = \frac{\partial}{\partial x}\left(D_e\varepsilon_e^b\frac{\partial c_e(x,t)}{\partial x}\right) + a_s(1-t_+^0)j_{Li}(x,t)$	(2a)
Boundary conditions	$\left.\frac{\partial c_e(x,t)}{\partial x}\right\|_{x=0} = 0, \left.\frac{\partial c_e(x,t)}{\partial x}\right\|_{x=L} = -\frac{I_{app}(t)}{A_{surf}}\frac{(1-t_+^0)}{D_e\varepsilon_e^b F}$	(2b)
Specific interfacial surface area	$a_s = \frac{3\varepsilon_s}{R_s}$	(2c)
Potential in solid phase	$\frac{\partial}{\partial x}\left(\sigma_s\varepsilon_s\frac{\partial\phi_s(x,t)}{\partial x}\right) = a_s F j_{Li}(x,t)$	(3a)
Boundary conditions	$\sigma_s\varepsilon_s\left.\frac{\partial\phi_s(x,t)}{\partial x}\right\|_{x=0} = \frac{I_{app}(t)}{A_{surf}}$ $\left.\frac{\partial\phi_s(x,t)}{\partial x}\right\|_{x=\delta_{pos}} = \phi_s(x,t)\|_{x=L} = 0$	(3b)
Potential in electrolyte phase	$\frac{\partial}{\partial x}\left(\kappa_e\varepsilon_e^b\frac{\partial\phi_e(x,t)}{\partial x} + \kappa_e\varepsilon_e^b\nu\frac{2RT}{F}\frac{\partial \ln c_e(x,t)}{\partial x}\right) = -a_s F j_{Li}(x,t)$	(4a)
Boundary conditions	$\left.\frac{\partial\phi_e(x,t)}{\partial x}\right\|_{x=0} = \phi_e(x,t)\|_{x=L} = 0$	(4b)
Butler-Volmer equation	$j_{Li}(x,t) = \frac{i_0(x,t)}{F}\left(\exp\left(\alpha_a\frac{F}{RT}\eta(x,t)\right) - \exp\left(\alpha_c\frac{F}{RT}\eta(x,t)\right)\right)$	(5a)
Electrode overpotential	$\eta(x,t) = \phi_s(x,t) - \phi_e(x,t) - U(x,t) - R_f j_{Li} F$	(5b)
Exchange current density	$i_0(x,t) = k_0(c_e(x,t))^{\alpha_a}\left(c_s^{max} - c_s^{surf}(x,t)\right)^{\alpha_a}\left(c_s^{surf}(x,t)\right)^{\alpha_c}$	(5c)
Cell voltage	$V(t) = \phi_s(0,t) - \phi_s(L,t) - \frac{R_{cc}}{A_{surf}} I_{app}(t)$	(6)

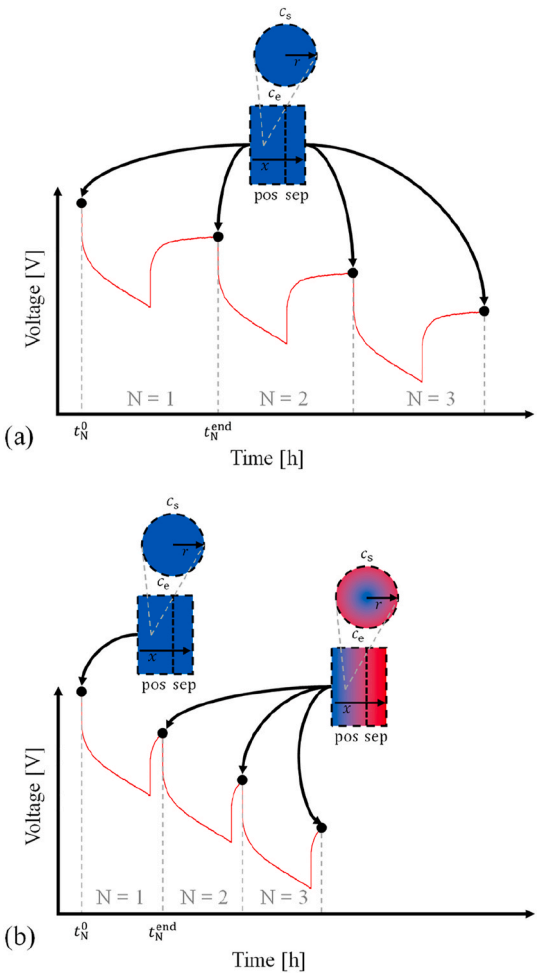


Fig. 2. Schematic illustration of the standard (discharge) GITT measurement method (a), and the accelerated GITT measurement method (b) for determining D_s and k_0 in combination with parameter optimization in the DFN model.

measurements are time-consuming, which in addition might lead to increased battery aging, self-discharge, or failure. This, in turn, slows down the development process and increases the costs of battery development.

2.3.2. Accelerated method

The accelerated and standard methods use the same parameter-identification procedure, as described in Section 2.3.1 and in the section "Parameter optimization algorithm" of the SI. They differ only in the relaxation duration and the treatment of the initial concentration fields at the start of each pulse interval. For each GITT pulse N, comprising the current pulse and subsequent relaxation period, one parameter pair ($D_{s,N}$, $k_{0,N}$) is determined and associated with the initial lithiation degree χ_N. Both parameters are held constant within that interval but may change between intervals. Thus, the procedure provides discrete pulse-wise parameter estimates; global continuous functions $D_s(\chi)$ and $k_0(\chi)$ are not optimized.

At the first pulse (N = 1), c_s is estimated based on the initial voltage (e.g., 4.3 V) and c_e on the initial electrolyte concentration ($c_{e,0}$). At this point, the cell is assumed to be under equilibrium conditions, as shown by the blue-colored schematic half-cell in Fig. 2b. For all pulses after the first (N > 1), the complete spatial concentration fields of c_s and c_e are taken from the DFN model or ESPM at the final time step of the previous pulse (t_{end}^{N-1}) and used as initial conditions for the pulse under investigation, which can be represented for c_s and c_e with

$$c_s\left(x, r, t_0^N\right) = c_s\left(x, r, t_{end}^{N-1}\right), \text{for N} > 1 \tag{9a}$$

$$c_e\left(x, t_0^N\right) = c_e\left(x, t_{end}^{N-1}\right), \text{for N} > 1 \tag{9b}$$

respectively. In Eq. (9), t_0^N is first time step of the N-th pulse. At the interval boundary, the concentration fields are transferred without modification. The values $D_{s,N}$ and $k_{0,N}$ are then optimized for the subsequent interval using this initial state, without reoptimizing previously fitted intervals. Because the relaxation duration is shorter in the accelerated method, neither c_s nor c_e reaches a steady state, leading to the formation of concentration gradients, as illustrated by the blue-to-red color transitions in the schematic half-cell shown in Fig. 2b.

Compared to the standard method, the primary advantage of the accelerated method is the substantial reduction in experimental time, enabling faster parameterization. However, the electrode equilibrium-potential curve must be determined independently because the shortened relaxation periods do not provide sufficiently relaxed voltage values from which this curve can be obtained directly.

In this work, the electrode equilibrium-potential curve over the full investigated lithiation range was determined by extrapolating discharge voltage curves measured at several relatively low C-rates to zero current [25], as shown in Fig. S1d. The corresponding measurements required a total test duration of 115 h. Compared with the discrete equilibrium-potential values obtained from standard GITT measurements, this extrapolation provides a smoother curve, particularly near the cutoff limits. More details about the method for determining the equilibrium potential curve with extrapolation to zero current can be found in Refs. [25–28].

2.4. Model implementation and settings

Spatial and temporal discretization methods were applied to solve the PDEs described in Eqs. (1)–(4). The finite difference method was used to discretize Eq. (1) along the *r*-direction, while the finite volume method was employed for Eqs. (3) and (4) along the *x*-direction. Using node optimization, the electrode and particle domains were discretized into 18 nodes, while the separator region was discretized with 9 nodes. Further details regarding node optimization are provided in the SI under the "Node optimization" Section. For the DFN, the system of differential-algebraic equations was efficiently solved using Newton's method [20] with a tolerance set to 1×10^{-3} for all simulations. For all simulations, the time step was set to 1 s and the model operated under isothermal conditions at 25 °C. Model programming and simulations were carried out using MATLAB R2024a. A computer with AMD Ryzen 7 5700 U CPU @ 1.8 GHz, 24 GB RAM and Windows operating system has been used.

3. Experimental

Half-cell measurements were performed using coin cells (CR2032). The configuration consisted of a disc-shaped positive electrode with a diameter of 12 mm, composed of $LiNi_{0.4}Co_{0.6}O_2$ (NC46), cut from a commercial battery (RouteJade) with a nominal cell capacity of 2.1 Ah. The nominal areal capacity of the harvested positive electrode was approximately 1.68 mAh cm^{-2}. The C-rates reported below are approximate and were calculated using this nominal areal capacity. The average particle size was determined by analyzing 2D top-down scanning electron microscopy (SEM) images using ImageJ software [29]. Fig. S1e presents a cross-sectional SEM image of the electrode. A Li-metal foil with a diameter of 14 mm was used as the counter electrode and an 18 mm diameter separator (Celgard 2325) was placed between the positive and counter electrode. The cells were filled with 50 µL of 1M lithium hexafluorophosphate (LiPF6) dissolved in a 50/50 (v/v) mixture of ethylene carbonate (EC) and ethyl methyl carbonate (EMC) and assembled in an argon-filled glove box. Following assembly, the cells were left to rest for 24 h before undergoing two formation cycles, using

CC (dis)charging at 0.18 mA cm^{-2} (approximately 0.11C) between 4.3 V and 3 V, with a 30 min rest between (dis)charging. This was succeeded by two activation cycles at 0.34 mA cm^{-2} (approximately 0.20C), involving CC-constant voltage (CV) (dis)charging to 4.3 and 3 V with a cut-off current of 0.04 mA cm^{-2} and a 1 h rest duration between (dis) charging. Before performing the discharge GITT measurements, the cells were rested for 6 h to ensure they reached an equilibrium state. All measurements were performed in a temperature chamber with the temperature set to 25 °C.

Four discharge GITT measurements were performed, each with a different relaxation duration (6 h, 1 h, 10 min, and 1 min). Each GITT measurement consisted of 50 pulses between 4.3 V and 3 V, with pulse durations of 10 min under CC-discharging at 0.34 mA cm^{-2}, followed by the respective relaxation duration. Each pulse therefore discharged 0.0567 mAh cm^{-2}, corresponding to an average normalized lithiation increment of approximately $\Delta\chi = 0.012$, or 1.2 % of the investigated lithiation range; within this interval, D_s and k_0 are assumed to be locally constant. The total GITT measurement time for pulse relaxation duration of 6 h, 1 h, 10 min, and 1 min was 369 h, 69.7 h, 19.6 h and 10.7 h, respectively. The full GITT measurements for various relaxation durations are shown in Fig. S2. All measurements were performed using a commercial multichannel potentiostat (Biologic EC-Lab, France) in combination with a commercial temperature chamber (Memmert GmbH, Germany).

4. Results and discussion

4.1. Parameterization

Fig. 3a and b shows the determined D_s and k_0 as function of lithiation degree for GITT measurements with pulse relaxation durations of 6 h, 1 h, 10 min, and 1 min. The values for the 6 h relaxation duration were obtained using the standard method from previous work [17], while those for the shorter relaxation durations were determined using the accelerated method introduced in this work. All curves in Fig. 3a and b shows a similar magnitude and trend, except for the 1 min relaxation duration, which particularly deviates between lithiation degrees of 0.6 and 0.75 for D_s and 0.25 and 0.65 for k_0. The values obtained from the 6 h relaxation duration are assumed to be the most accurate, as the relatively long relaxation time is sufficient to reach full equilibrium. In this work, the 6 h curve is therefore used as a reference.

To assess the impact of shorter relaxation durations, the average differences between the parameters obtained at different relaxation durations were compared to the 6 h values, as shown with the blue bars in Fig. 3c. For D_s, the 1 h and 10 min relaxation durations show reasonable average differences of 15 % and 18 %, respectively. However, the 1 min measurement shows a far higher deviation of 44 % in average. The difference based on lithiation degree for D_s is shown in Fig. S3a. The average differences for k_0 (Fig. 3c, red bars) show a similar trend to those of D_s. The 1 h and 10 min measurements show the smallest deviations compared to the 6 h values, with average differences of 8 % and 16 %, respectively. The 1 min measurement shows a significantly larger deviation, with a 47 % average difference compared to the 6 h values. The difference based on lithiation degree for k_0 is shown in Fig. S3b. It can therefore be concluded that 1 min relaxation durations produce D_s and k_0 estimates with substantially larger deviations from the 6 h reference.

The relaxation period in GITT measurements is dominated by diffusion-driven voltage relaxation, during which the diffusion overpotential governs the temporal voltage response and therefore provides the primary information required to estimate D_s through the optimization procedure, as discussed by Ali et al. [17]. When the relaxation duration is too short, this diffusion-controlled regime is insufficiently captured, resulting in poor identifiability of D_s. The associated incomplete concentration relaxation is evident from the solid- and electrolyte-phase concentration ratios, ($c_{s,min}/c_{s,max}$ and $c_{e,min}/c_{e,max}$), respectively, at the end of each rest period (Fig. S4), where values approaching 100 % indicate increasing spatial uniformity. At a lithiation degree of 0.67, both ratios remain close to 100 % after a 6 h rest but decrease to approximately 90 % and 98.7 %, respectively, after a 1 min rest, indicating a substantial residual solid-phase concentration gradient and a residual electrolyte-phase concentration gradient.

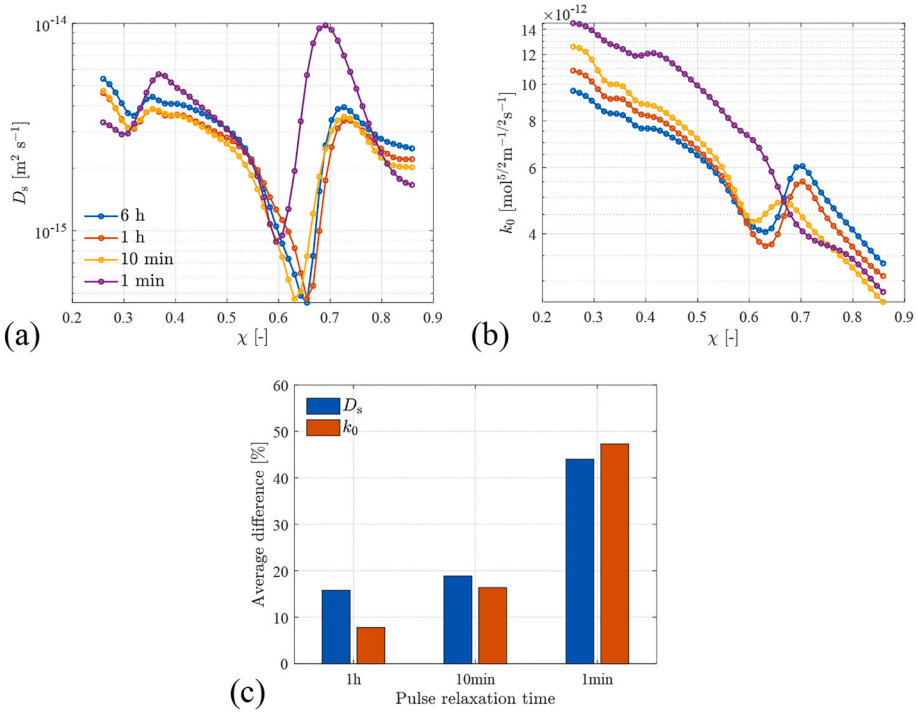


Fig. 3. Results of the determined D_s (a) and k_0 (b) for GITT relaxation durations of 6 h, 1 h, 10 min, and 1 min as a function of lithiation degree. The average absolute percentage differences of D_s and k_0 between the 6 h (reference) and the other relaxation durations (c).

Consequently, the optimization algorithm compensates for the incorrectly estimated diffusion behavior by adjusting k_0, leading to parameter combinations that reproduce the measured voltage reasonably well (Fig. 4d), without causing large apparent fitting errors, although the inferred D_s and k_0 values deviate substantially from the 6 h reference profiles. This deviation of D_s then propagates to incorrect initial values of c_s and c_e at step $N+1$, triggering a domino effect that increases the deviations in the estimated D_s and k_0 for subsequent pulses. In contrast, a 10 min relaxation duration produces estimates that remain substantially closer to the 6 h reference profiles. This highlights the importance of allowing sufficient relaxation duration in GITT experiments to ensure reliable parameter estimation for the accelerated method. However, this also suggests that the relaxation duration can be shortened compared to standard relaxation durations used in the literature, which averages 3.5 h [6–8,11,12,30,31] for estimating D_s and k_0, enabling shorter measurement time.

4.2. Validation

Full CC-discharge validations measurements were performed at current densities of 0.34, 1.00, and 1.68 mA cm^{-2} on the same cell. Fig. 4a shows the voltage discharge curves for both the measured (symbols) and simulated (lines) data using the D_s and k_0 values derived from the 6 h relaxation durations. The validation demonstrates good agreement with the measured data, with errors remaining within the ±30 mV range, except in the low-voltage region. Fig. 4b shows simulation results obtained using D_s and k_0 values derived from the 1 h

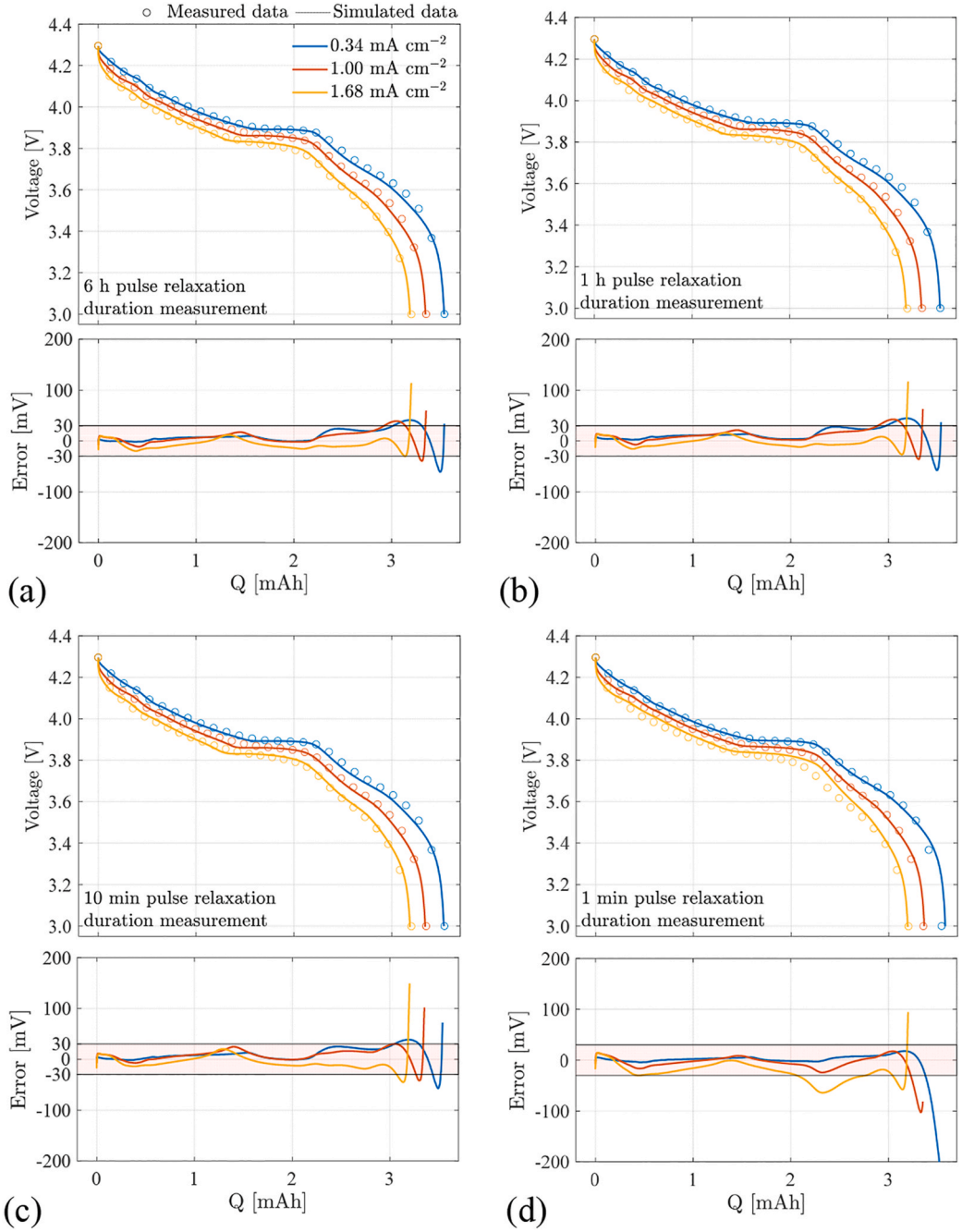


Fig. 4. Simulated data (solid lines) compared to measured data (symbols) for CC-discharging at various current densities, for D_s and k_0 determined using 6 h (a), 1 h (b), 10 min (c) and 1 min (d) GITT relaxation durations. The error between simulated and measured data is shown below each plot.

relaxation durations, which are similar to those obtained using values from 6 h relaxation durations. Fig. 4c shows validation results with D_s and k_0 obtained using the 10 min relaxation duration for the same CC-discharge current densities. Since the D_s and k_0 values derived from this shorter relaxation time are close to those obtained from the 6 h relaxation time, as shown in Section 4.1, the validation results show similar accuracy compared to the 6 h reference. The simulated data again aligns well with the measured data, with errors within the ±30 mV range. Fig. 4d shows the simulation results based on the D_s and k_0 derived from the 1 min relaxation duration. Noticeable deviations emerge, particularly in the mid-to-low voltage range, where the agreement between simulation and measurement progressively deteriorates. While the overall voltage response is still reproduced reasonably well, these deviations are consistent with the previously discussed propagation of parameter errors: small deviations of the D_s estimates from the 6 h reference during the early GITT pulses lead to incorrect initial concentration states for subsequent pulses, causing a gradual accumulation of error toward higher lithiation degrees. As a result, the fitted parameter sets continue to provide an acceptable voltage match, but the underlying D_s and k_0 values increasingly deviate from the 6 h reference profile, as already indicated by the comparison in Fig. 3.

Fig. 5 compares the measured and simulated voltage responses during a dynamic load profile (Worldwide Harmonised Light vehicles Test Procedure (WLTP) cycle) for D_s and k_0 parameters derived from different pulse relaxation durations: (a) 6 h, (b) 1 h, (c) 10 min, and (d) 1 min. The current density as a function of the time is shown in Fig. 5e, with a mean discharge current density of 1.4 mA cm^{-2}. Across all four cases, the model demonstrates high fidelity in capturing the transient behavior under the dynamic current load with the absolute error generally remaining well within the 30 mV boundary during both current loading conditions (0-30 min) and subsequent relaxation (30-45 min). Reducing the relaxation duration from 6 h down to 10 min results in only minor deviations in voltage prediction, confirming that shorter GITT relaxation measurements retain sufficient D_s and k_0 estimation capability while reducing GITT measurement time.

The RMSE values representing the simulation errors compared to the measurements in Figs. 4 and 5 are shown in Table 2. The RMSEs show that the simulations with D_s and k_0 derived from the 6 h relaxation duration closely match the experimental data, with RMSE values ranging from 5.5 mV to 17.7 mV and a mean RMSE of 12.6 mV. For 1 h relaxation duration derived from D_s and k_0, with RMSE values ranging from 5.6 mV to 17.7 mV and a mean RMSE of 12.7 mV, corresponding to 0.8 % higher than the 6 h reference. Similarly, the RMSE values for the 10 min relaxation duration range from 5.6 mV to 17.4 mV across the different applied current densities, with a mean RMSE of 13.2 mV, corresponding to 4.8 % higher than the 6 h reference. The 1 min relaxation duration shows the largest voltage simulation error, with a mean RMSE of 21.4 mV, corresponding to 69.8 % higher than the 6 h reference. These results indicate that the shorter relaxation duration leads to a noticeable reduction in simulated accuracy compared to longer relaxation times. However, despite the increased RMSE, the overall agreement between simulation and measurement remains qualitatively reasonable, indicating that voltage-based metrics alone are not sufficient to establish the physical accuracy or uniqueness of the identified parameters. In combination with the parameter deviations observed in Fig. 3, this suggests that the 1 min relaxation duration leads to parameter sets that reproduce the voltage response to an acceptable extent but deviate substantially from the 6 h reference profiles. In contrast, a 10 min relaxation time appears to provide a more reliable basis to obtain reliable parameter estimates, offering accuracy comparable to the 6 h reference but with reduced measurement time.

It is important to highlight a limitation of the sequential local fitting procedure under extremely short rest conditions, such as the 1 min relaxation protocol. The fundamental assumption of this localized workflow is that D_s and k_0 remain constant during the single pulse interval. However, when the rest time is insufficient, the inherited concentration gradients inside the solid phase become excessively large and complex. In reality, D_s and k_0 varies continuously with the local lithiation degree across the particle radius. By forcing a single, locally constant D_s and k_0 operator onto a highly distorted, non-equilibrium concentration profile, the physical assumption breaks down. The optimization algorithm is then forced to overcompensate for these severe mathematical discrepancies by generating unphysical values for both D_s and k_0 as observed by the stark deviations in the 1 min protocol results (Fig. 3a and b).

4.3. Voltage relaxation-rate threshold and reduced-order model

In Section 4.1, a simplified approach was used to determine D_s and k_0, based on a fixed relaxation duration. The approach introduced in this section involves a more advanced method, which is based on relaxation (-rate) behavior. Depending on the battery design, electrode materials, lithiation degree and measurements conditions (e.g., measurement temperature and the applied pulse current density), the relaxation duration required for obtaining D_s and k_0 estimates that remain sufficiently close to the operational reference may vary. This variability introduces uncertainty in selecting the appropriate relaxation duration.

A more effective approach to address this issue is to define relaxation in terms of a relaxation-rate threshold, using voltage change over time rather than a fixed duration (e.g., hours, minutes, or seconds). Using the same relaxation-rate threshold provides a consistent operational termination criterion, regardless of variations in relaxation behavior under different conditions. In contrast, a fixed relaxation duration does not adapt to state-dependent relaxation kinetics, which can lead to poor parameter identifiability if insufficient time is allowed to capture the diffusion dynamics. The relaxation behaviour underlying this effect is shown in Fig. 6a, which shows the voltage response (blue line) during a representative GITT pulse together with the corresponding relaxation rates (red symbols), starting from an initial lithiation degree of 0.52. Fig. 6b compares these relaxation-rates thresholds across a range from 100 to 0.01 mV h^{-1}, corresponding to relaxation durations from 0.1 to 76.9 min.

To determine the suitable relaxation-rate threshold, D_s and k_0 were determined by mathematical optimization at different relaxation-rate thresholds, following the parameter optimization procedure explained in Section 2.3 and Ref. [17]. The results are compared to those obtained at the threshold of 0.01 mV h^{-1}, which corresponds to relaxation durations greater than 1 h, and is used as the operational reference for the relaxation-rate analysis, consistent with the results in Section 4.2. Fig. 6c shows the D_s estimates obtained at different relaxation-rate thresholds. The difference relative to the reference value obtained at 0.01 mV h^{-1} increases rapidly for thresholds greater than 10 mV h^{-1}, as indicated by the red dashed line. Therefore, under the tested operating conditions, a relaxation rate threshold of 10 mV h^{-1} provides a suitable trade-off: it reduces the measurement time, while the corresponding D_s estimate differs by 2.7 % from that obtained using the reference threshold of 0.01 mV h^{-1}. A similar conclusion can be drawn for k_0, as shown in Fig. 6d, where the difference between the values at 10 mV h^{-1} and 0.01 mV h^{-1} is just 0.03 %. This indicates that the influence of k_0 during relaxation is minimal. The results show similar conclusion at a lithiation degree of 0.7, of which the results are shown in Fig. S5. The results align well with the previous work [17], as k_0 is optimum to be estimated in the initial stage of the applied pulse, where it predominates over other overpotentials, associated with electrolyte processes and D_s. However, it is important to note that these specific thresholds may be sensitive to cell chemistry, temperature, and operating conditions. The optimal rate likely varies across different battery systems, necessitating further research to evaluate the broader generality of this approach.

When relaxation-rate thresholds exceed approximately 10 mV h^{-1}, the diffusion-controlled relaxation regime is no longer sufficiently resolved, leading to D_s estimates that increasingly deviate from the

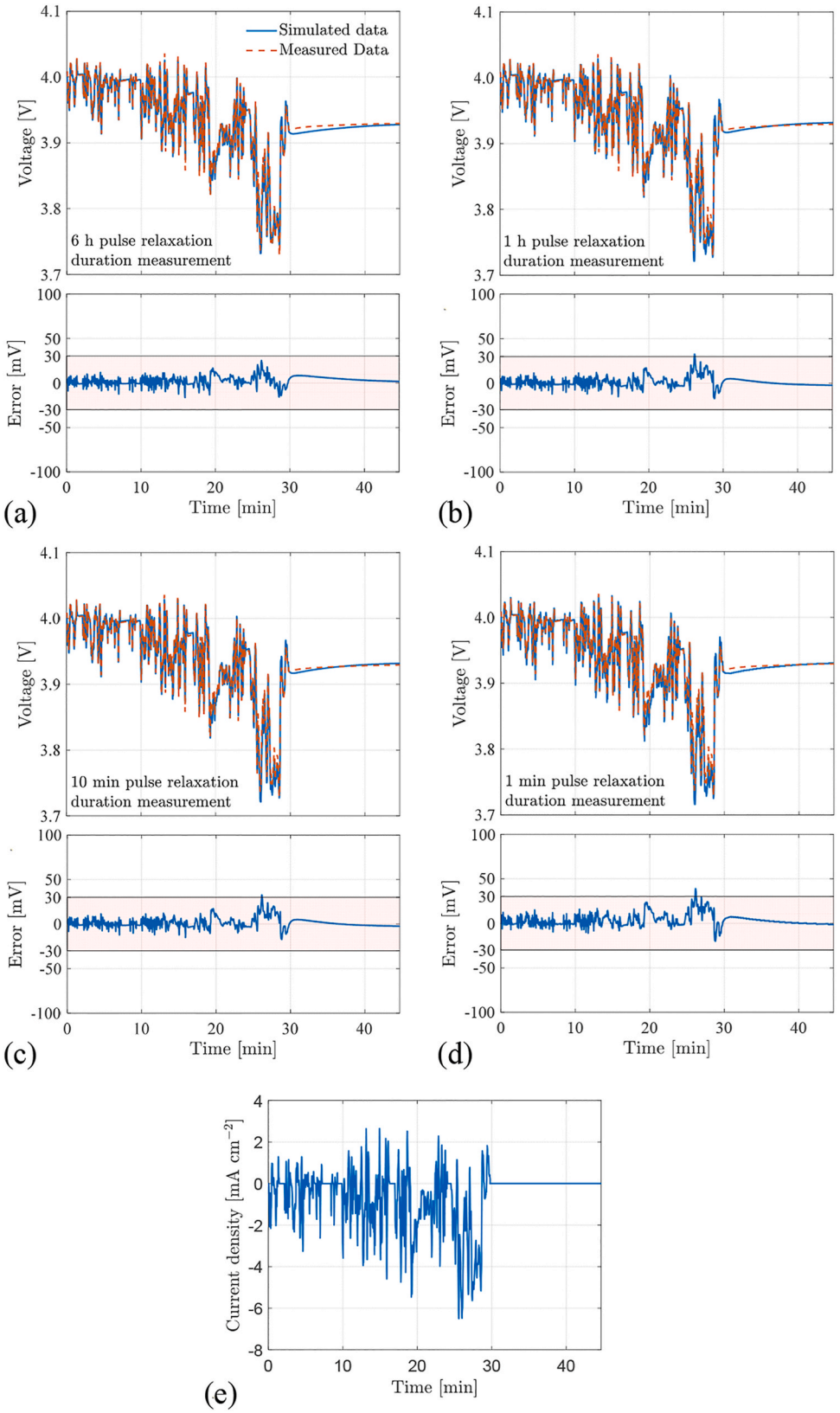


Fig. 5. Simulated data (solid lines) compared to measured data (symbols) for the WLTP load profile, for D_s and k_0 determined using 6 h (a), 1 h (b), 10 min (c) and 1 min (d) GITT relaxation durations. The error between simulated and measured data is shown below each plot. Current density as a function of time that was applied to the model (e).

Table 2
RMSE values corresponding to the simulation errors in Figs. 4 and 5, evaluated at various CC-discharge current densities and the WLTP drive cycle, respectively.

Pulse relaxation duration	RMSE [mV]				
	0.34 mA cm^{-2}	1.00 mA cm^{-2}	1.68 mA cm^{-2}	WLTP	Mean
6 h	17.7	14.8	12.3	5.5	12.6
1 h	17.7	14.7	12.9	5.6	12.7
10 min	17.4	14.5	15.3	5.6	13.2
1 min	30.0	18.1	30.0	7.5	21.4

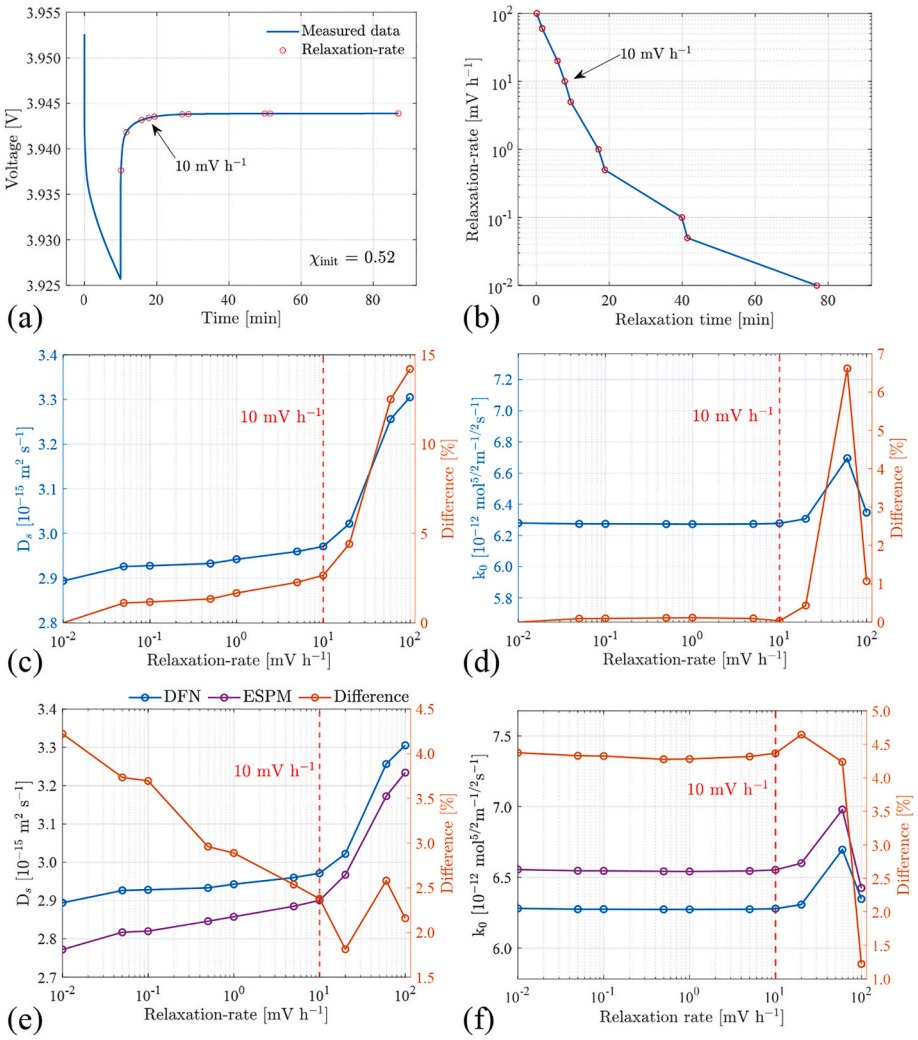


Fig. 6. GITT voltage pulse (blue solid line) and various relaxation-rates (red symbols) after the applied current pulse (a) and corresponding relaxation-rate as a function of time (b). Comparison of various relaxation-rates for obtaining D_s (c) and k_0 (d). Comparison between the DFN model and ESPM for determining D_s (e) and k_0 (f) at different relaxation-rates. The dashed red line indicates the 10 mV h^{-1} relaxation-rate (c-f).

reference. As discussed in Sections 4.1 and 4.2, such deviations in D_s subsequently affect the estimation of k_0, since the optimization compensates for the incorrect diffusion behaviour by adjusting the kinetic parameter to maintain agreement between simulation and measurement. Consequently, although the direct sensitivity of the relaxation period to k_0 is limited, the increasing deviation of D_s at higher relaxation-rate thresholds indirectly leads k_0 values that deviate from the reference values through parameter coupling in the optimization procedure.

In terms of the total GITT measurement duration, a comparison was made between the different fixed relaxation durations and voltage relaxation-rate thresholds, as shown in Table 3. The total GITT measurement duration for 50 pulses using a 6 h relaxation duration after each applied current pulse is 309 h (Fig. S2a). Using a voltage relaxation-rate threshold of 0.01 mV h^{-1} reduces the GITT measurement duration to 117 h, corresponding to a reduction of 62 % relative to the 6 h protocol. When using the selected relaxation-rate threshold of 10 mV h^{-1}, the GITT measurement duration is further reduced to 16 h, corresponding to a reduction of 95 % relative to the 6 h protocol. These values refer only to the GITT component of the workflow. The independent determination of the equilibrium-potential curve by zero-current extrapolation required an additional 115 h (see Section 2.3.2). Consequently, when the equilibrium-potential determination is included, the complete accelerated workflows using thresholds of 0.01 and 10 mV h^{-1} require 232 and 131 h, respectively, corresponding to overall reductions of 25 % and 58 % relative to the self-contained 309 h

Table 3
Calculated GITT measurement duration and complete workflow duration for 50 current pulses of 10 min duration, using different fixed relaxation durations or voltage relaxation-rate thresholds.

Pulse relaxation duration/rate threshold	GITT measurement duration [h]	Reduction in GITT duration relative to 6 h [%]	Total workflow time [h] (Overall reduction [%])
6 h	309	-	309 (–)[a]
0.01 mV h^{-1}	117	62	232 (25 %)[b]
10 mV h^{-1}	16	95	131 (58 %)[b]

[a] For the conservative workflow comparison, the standard 6 h GITT protocol is treated as a self-contained measurement providing both the equilibrium-potential data and the data for parameter estimation.

[b] For the accelerated protocols, the complete workflow duration reported here includes the additional 115 h required for independent determination of the equilibrium-potential curve by zero-current extrapolation.

standard GITT protocol.

It is important to note that applying a fixed voltage relaxation-rate threshold results in relaxation durations that vary depending on the degree of lithiation. The relaxation duration of each pulse at 0.01 mV h^{-1} and 10 mV h^{-1} is shown in Fig. S6a–b, respectively. From these observations, the relaxation time for 10 mV h^{-1} shows a similar behavior, although inverted, compared to the obtained D_s in Fig. 3a. This suggests that the relaxation-rate is heavily influenced by D_s, and that the trend in D_s can be predicted if the correct relaxation-rate is used.

In an effort to further accelerate the estimation process of D_s and k_0, a comparison was made between the DFN model and the ESPM at various relaxation-rates, as shown in Fig. 6e and f. The results show that the difference between the two models is small, with only a 2.3 % average difference for D_s and a difference for k_0 (4.3 %) when comparing at a relaxation-rate threshold of 10 mV h^{-1}. These results show that the ESPM can be used to determine D_s and k_0 with only small differences relative to the DFN results at 10 mV h^{-1}, while reducing the computational effort compared to the DFN model.

5. Conclusions

This study introduces an approach to accelerate GITT measurements for determining D_s and k_0, addressing the issue of lengthy measurement durations traditionally associated with this method. The results demonstrate that close agreement with the operational reference estimates and significantly shorter measurement times can be achieved using this new accelerated approach, which uses the DFN model to resolve local state variables during battery operation. Validation shows that the accelerated method, employing a 10 min rest duration, produces D_s and k_0 estimates close to those obtained using the 6 h reference protocol and comparable voltage RMSE values, while the reference protocol requires a 6 h rest duration after each pulse. Additionally, while this study focuses on discharge GITT measurements, the method could potentially be extended to charging conditions.

Furthermore, the use of a voltage relaxation-rate threshold instead of a fixed relaxation duration allows the rest period to adapt to the observed voltage-relaxation behavior. A voltage relaxation-rate threshold of 10 mV h^{-1} was identified as a practical termination criterion for the investigated cell design/chemistry, temperature and test protocol, reducing the GITT measurement duration by 95 %, from 309 to 16 h, compared with the standard protocol using a 6 h relaxation period after each GITT pulse. Including the additional 115 h required for the independent determination of the equilibrium-potential curve, the complete initial accelerated workflow requires 131 h, corresponding to an overall reduction of approximately 58 % relative to the self-contained 309 h standard GITT protocol.

Additionally, the study compared the performance of the ESPM with the DFN model. The ESPM demonstrated its potential to replace the DFN model for optimizing D_s and k_0, requiring less computational effort while producing parameter estimates close to the DFN results. It should be noted that these results are specific to the chemistry used in this study. The suitable relaxation-rate threshold may vary depending on cell chemistry, temperature, and other operating conditions. Therefore, further research is needed to evaluate the generality of this approach and to identify the most suitable relaxation-rate threshold for different battery chemistries and conditions. Furthermore, it should be noted that the conclusions and parameter estimation framework presented in this work apply specifically to solid-solution active materials.

Overall, these findings show that GITT measurements and parameter optimization for D_s and k_0 can be conducted much more efficiently in terms of both measurement time and computational effort. This facilitates faster cell parameterization and may enable more frequent GITT measurements in ageing studies, supporting the investigation of changes in the effective D_s and k_0 during ageing.

CRediT authorship contribution statement

Haider Adel Ali Ali: Writing – review & editing, Writing – original draft, Visualization, Methodology, Investigation, Data curation, Conceptualization. **Luc H.J. Raijmakers:** Writing – review & editing, Writing – original draft, Visualization, Supervision, Resources, Project administration, Funding acquisition, Conceptualization. **Anna Windmüller:** Writing – review & editing. **Hermann Tempel:** Supervision, Project administration, Funding acquisition. **Boryann Liaw:** Writing – review & editing. **Peter H.L. Notten:** Writing – review & editing. **Rüdiger-A. Eichel:** Writing – review & editing, Supervision, Resources, Project administration, Funding acquisition.

Declaration of competing interest

The authors declare that they have no known competing financial interests or personal relationships that could have appeared to influence the work reported in this paper.

Acknowledgments

The authors thank their colleagues at Forschungszentrum Jülich GmbH for their great support. This study has been developed in the LLEC::VxG and ALIBES projects, which are funded by the German Federal Ministry of Education and Research, Technology and Space under Grant No. 03SF0628 and 13XP0530B, respectively.

Appendix A. Supplementary data

Supplementary data to this article can be found online at https://doi.org/10.1016/j.jpowsour.2026.241495.

Nomenclature			
A_{surf}	Electrode surface area, m^2	t_{end}^N	Last time step of the N-pulse, s
a_s	Specific interfacial surface area, m^{-1}	t_+^0	Transference number, -
b	Bruggeman exponent, -	U	Equilibrium potential of the electrode, V
c_e	Concentration in the electrolyte-phase, mol m^{-3}	V	Cell voltage, V
$c_{e,0}$	Initial electrolyte concentration, mol m^{-3}	x	Position across cell layers, m
c_s	Concentration in the solid-phase, mol m^{-3}	Greek	
c_s^{max}	Maximum concentration in the solid-phase, mol m^{-3}	α_a	Anodic charge-transfer coefficient, -
c_s^{surf}	Surface concentration in the solid-phase, mol m^{-3}	α_c	Cathodic charge-transfer coefficient, -
D_e	Electrolyte-phase diffusion coefficient, m^2 s^{-1}	δ	Thickness, m
D_s	Solid-phase diffusion coefficient, m^2 s^{-1}	ε_e	Electrolyte volume fraction, -
F	Faraday constant, 96487 C mol^{-1}	ε_s	Active material volume fraction, -
$f_\pm$	Mean molar activity coefficient of the electrolyte, -	η	Electrode overpotential, V
i_0	Exchange current density, A m^{-2}	κ_e	Electrolyte ionic conductivity, S m^{-1}
I_{app}	Applied current, A	ν	Thermodynamic factor, -
j_{Li}	Molar ionic flux, mol m^{-2} s^{-1}	σ_s	Solid-phase electronic conductivity, S m^{-1}
k_0	Reaction-rate constant, $mol^{5/2}$ $m^{-1/2}$ s^{-1}	ϕ_e	Electrolyte-phase potential, V
L	Overall thickness of the cell, m	ϕ_e^{mean}	Mean electrolyte-phase potential, V
N	Pulse Number, -	ϕ_s	Solid-phase potential, V
Q	Capacity, Ah	χ	Lithiation degree, -
R	Universal gas constant, 8.314 J mol^{-1} K^{-1}	Abbreviations	
r	Radial position across a spherical particle, m	CC	Constant current
R_{cc}	Contact resistance, Ω m^2	CV	Constant voltage
R_s	Particle radius, m	DFN	Doyle-Fuller-Newman
R_f	Film resistance, Ω m^2	ESPM	Extended single particle model
T	Temperature, K	GITT	Galvanostatic intermittent titration technique
t	Time, s	LIB	Li-ion battery
t_0^N	First time step of the N-pulse, s	pos	Positive electrode
		sep	Separator

Data availability

Data will be made available on request.

References

[1] K. Kumaresan, G. Sikha, R.E. White, Thermal model for a Li-Ion cell, J. Electrochem. Soc. 155 (2007) A164, https://doi.org/10.1149/1.2817888.

[2] M. Doyle, J. Newman, A.S. Gozdz, C.N. Schmutz, J.-M. Tarascon, Comparison of modeling predictions with experimental data from plastic lithium ion cells, J. Electrochem. Soc. 143 (1996) 1890, https://doi.org/10.1149/1.1836921.

[3] V. Ramadesigan, P.W.C. Northrop, S. De, S. Santhanagopalan, R.D. Braatz, V. R. Subramanian, Modeling and simulation of lithium-ion batteries from a systems engineering perspective, J. Electrochem. Soc. 159 (2012) R31, https://doi.org/10.1149/2.018203jes.

[4] J. Newman, W. Tiedemann, Porous-electrode theory with battery applications, AIChE J. 21 (1975) 25–41, https://doi.org/10.1002/aic.690210103.

[5] Z. Chen, D.L. Danilov, R.-A. Eichel, P.H.L. Notten, Porous electrode modeling and its applications to Li-Ion batteries, Adv. Energy Mater. 12 (2022) 2201506, https://doi.org/10.1002/aenm.202201506.

[6] J. Schmalstieg, C. Rahe, M. Ecker, D.U. Sauer, Full cell parameterization of a high-power lithium-ion battery for a physico-chemical model: part I. Physical and electrochemical parameters, J. Electrochem. Soc. 165 (2018) A3799, https://doi.org/10.1149/2.0321816jes.

[7] C. Schmitt, M. Gerle, D. Kopljar, K.A. Friedrich, Full parameterization study of a high-energy and high-power Li-Ion cell for physicochemical models, J. Electrochem. Soc. 170 (2023) 070509, https://doi.org/10.1149/1945-7111/ace1a7.

[8] M. Ecker, T.K.D. Tran, P. Dechent, S. Käbitz, A. Warnecke, D.U. Sauer, Parameterization of a physico-chemical model of a lithium-ion battery: I. Determination of parameters, J. Electrochem. Soc. 162 (2015) A1836, https://doi.org/10.1149/2.0551509jes.

[9] K. Chayambuka, M. Jiang, G. Mulder, D.L. Danilov, P.H.L. Notten, Physics-based modeling of sodium-ion batteries part I: experimental parameter determination, Electrochim. Acta 404 (2022) 139726, https://doi.org/10.1016/j.electacta.2021.139726.

[10] C.-H. Chen, F.B. Planella, K. O'Regan, D. Gastol, W.D. Widanage, E. Kendrick, Development of experimental techniques for parameterization of multi-scale lithium-ion battery models, J. Electrochem. Soc. 167 (2020) 080534, https://doi.org/10.1149/1945-7111/ab9050.

[11] K. Chayambuka, G. Mulder, D.L. Danilov, P.H.L. Notten, Determination of state-of-charge dependent diffusion coefficients and kinetic rate constants of phase changing electrode materials using physics-based models, Journal of Power Sources Advances 9 (2021) 100056, https://doi.org/10.1016/j.powera.2021.100056.

[12] D.W. Dees, S. Kawauchi, D.P. Abraham, J. Prakash, Analysis of the galvanostatic intermittent titration technique (GITT) as applied to a lithium-ion porous electrode, J. Power Sources 189 (2009) 263–268.

[13] Y.-C. Chien, H. Liu, A.S. Menon, W.R. Brant, D. Brandell, M.J. Lacey, Rapid determination of solid-state diffusion coefficients in Li-based batteries via intermittent current interruption method, Nat. Commun. 14 (2023) 2289, https://doi.org/10.1038/s41467-023-37989-6.

[14] L. Yin, Z. Geng, Y.-C. Chien, T. Thiringer, M.J. Lacey, A.M. Andersson, D. Brandell, Implementing intermittent current interruption into Li-ion cell modelling for improved battery diagnostics, Electrochim. Acta 427 (2022) 140888, https://doi.org/10.1016/j.electacta.2022.140888.

[15] A.E. Gümrükçüoğlu, J. Burridge, K. O'Regan, E. Kendrick, J.M. Foster, A fast and accurate method for inferring solid-state diffusivity in lithium-ion battery active materials, J. Energy Storage 153 (2026) 120831, https://doi.org/10.1016/j.est.2026.120831.

[16] J. Hörmann, Y. Kuhn, S. Hein, B. Horstmann, T. Danner, A. Latz, Understanding the role of microstructure in the extraction of solid-state diffusion coefficients by a 3D modeling approach, J. Electrochem. Soc. 173 (2026) 130503, https://doi.org/10.1149/1945-7111/ae7cb8.

[17] H.A.A. Ali, L.H.J. Raijmakers, A. Windmüller, H. Tempel, B. Liaw, P.H.L. Notten, R.-A. Eichel, Evaluating the determination of solid-phase diffusion and reaction-rate constant for Li-ion batteries, J. Energy Storage 132 (2025) 117628, https://doi.org/10.1016/j.est.2025.117628.

[18] A. Verma, K. Smith, S. Santhanagopalan, D. Abraham, K.P. Yao, P.P. Mukherjee, Galvanostatic intermittent titration and performance based analysis of LiNi0.5Co0.2Mn0.3O2 cathode, J. Electrochem. Soc. 164 (2017) A3380, https://doi.org/10.1149/2.1701713jes.

[19] D.S. Mebane, R. Jackowska, M.W. Fouts, F.B. Planella, E. Kendrick, M.R. Mehta, J. W. Lawson, Initial proof-of-concept for an accelerated galvanostatic intermittent titration technique via embedded machine learning, J. Electrochem. Soc. 172 (2025) 120527, https://doi.org/10.1149/1945-7111/ae26cd.

[20] H.A.A. Ali, L.H.J. Raijmakers, K. Chayambuka, D.L. Danilov, P.H.L. Notten, R.-A. Eichel, A comparison between physics-based Li-ion battery models, Electrochim. Acta 493 (2024) 144360, https://doi.org/10.1016/j.electacta.2024.144360.

[21] S.J. Moura, F.B. Argomedo, R. Klein, A. Mirtabatabaei, M. Krstic, Battery state estimation for a single particle model with electrolyte dynamics, IEEE Trans. Control Syst. Technol. 25 (2017) 453–468, https://doi.org/10.1109/TCST.2016.2571663.

[22] Z. Khalik, M.C.F. Donkers, H.J. Bergveld, Model simplifications and their impact on computational complexity for an electrochemistry-based battery modeling toolbox, J. Power Sources 488 (2021) 229427, https://doi.org/10.1016/j.jpowsour.2020.229427.

[23] F.B. Planella, W. Ai, A.M. Boyce, A. Ghosh, I. Korotkin, S. Sahu, V. Sulzer, R. Timms, T.G. Tranter, M. Zyskin, S.J. Cooper, J.S. Edge, J.M. Foster, M. Marinescu, B. Wu, G. Richardson, A continuum of physics-based lithium-ion battery models reviewed, Prog. Energy 4 (2022) 042003, https://doi.org/10.1088/2516-1083/ac7d31.

[24] A. Jokar, B. Rajabloo, M. Désilets, M. Lacroix, Review of simplified pseudo-two-dimensional models of lithium-ion batteries, J. Power Sources 327 (2016) 44–55, https://doi.org/10.1016/j.jpowsour.2016.07.036.
[25] F.S.J. Hoekstra, L.H.J. Raijmakers, M.C.F. Donkers, H.J. Bergveld, Comparison of battery electromotive-force measurement and modelling approaches, J. Energy Storage 56 (2022) 105910, https://doi.org/10.1016/j.est.2022.105910.
[26] D. Danilov, R.a.H. Niessen, P.H.L. Notten, Modeling all-solid-state Li-Ion batteries, J. Electrochem. Soc. 158 (2010) A215, https://doi.org/10.1149/1.3521414.
[27] N. Kazemi, D.L. Danilov, L. Haverkate, N.J. Dudney, S. Unnikrishnan, P.H. L. Notten, Modeling of all-solid-state thin-film Li-ion batteries: accuracy improvement, Solid State Ionics 334 (2019) 111–116, https://doi.org/10.1016/j.ssi.2019.02.003.
[28] D. Li, D.L. Danilov, L. Gao, Y. Yang, P.H.L. Notten, Degradation mechanisms of C6/LiFePO4 batteries: experimental analyses of cycling-induced aging, Electrochim. Acta 210 (2016) 445–455, https://doi.org/10.1016/j.electacta.2016.05.091.
[29] C.A. Schneider, W.S. Rasband, K.W. Eliceiri, NIH image to ImageJ: 25 years of image analysis, Nat. Methods 9 (2012) 671–675, https://doi.org/10.1038/nmeth.2089.
[30] A. Nickol, T. Schied, C. Heubner, M. Schneider, A. Michaelis, M. Bobeth, G. Cuniberti, GITT analysis of lithium insertion cathodes for determining the lithium diffusion coefficient at low temperature: challenges and pitfalls, J. Electrochem. Soc. 167 (2020) 090546, https://doi.org/10.1149/1945-7111/ab9404.
[31] J.S. Horner, G. Whang, D.S. Ashby, I.V. Kolesnichenko, T.N. Lambert, B.S. Dunn, A. A. Talin, S.A. Roberts, Electrochemical modeling of GITT measurements for improved solid-state diffusion coefficient evaluation, ACS Appl. Energy Mater. 4 (2021) 11460–11469, https://doi.org/10.1021/acsaem.1c02218.